Experimental evaluations of the microchannel flow model

K J Parker

Department of Electrical and Computer Engineering, University of Rochester, Hopeman Building 203, PO Box 270126, Rochester, NY, 14627-0126, USA

E-mail: kevin.parker@rochester.edu

Abstract

Recent advances have enabled a new wave of biomechanics measurements, and have renewed interest in selecting appropriate rheological models for soft tissues such as the liver, thyroid, and prostate. The microchannel flow model was recently introduced to describe the linear response of tissue to stimuli such as stress relaxation or shear wave propagation. This model postulates a power law relaxation spectrum that results from a branching distribution of vessels and channels in normal soft tissue such as liver. In this work, the derivation is extended to determine the explicit link between the distribution of vessels and the relaxation spectrum. In addition, liver tissue is modified by temperature or salinity, and the resulting changes in tissue responses (by factors of 1.5 or greater) are reasonably predicted from the microchannel flow model, simply by considering the changes in fluid flow through the modified samples. The 2 and 4 parameter versions of the model are considered, and it is shown that in some cases the maximum time constant (corresponding to the minimum vessel diameters), could be altered in a way that has major impact on the observed tissue response. This could explain why an inflamed region is palpated as a harder bump compared to surrounding normal tissue.

Keywords: biomechanics, viscoelasticity, shear waves, dispersion

(Some figures may appear in colour only in the online journal)

1. Introduction

An impressive number of techniques for estimating the elastic properties of tissues have been integrated into imaging systems in recent years (Parker *et al* 2011, Doyley 2012). These developments have spurred renewed interest in the identification of the most appropriate physical or mathematical models to predict and parameterize the behavior of tissues in shear wave

experiments (Klatt *et al* 2007) or stress relaxation (SR) measurements (Zhang *et al* 2007). Since there are many types of tissues and a great wealth of models from materials research (Fung 1981a, Delingette 1998, Liu and Bilston 2000, Walker *et al* 2000, Humphrey 2003, Bercoff *et al* 2004, Catheline *et al* 2004, Chen *et al* 2004, 2009, 2013a, 2013b, Gennisson *et al* 2006, Samani *et al* 2007, Giannoula and Cobbold 2009), there are numerous possibilities to evaluate. Some major categories include the traditional spring and dashpot models (Fung 1981a), the power law and fractional derivative models (Caputo 1967, Bagley and Torvik 1983, Suki *et al* 1994, Taylor *et al* 2001, Kiss *et al* 2004, Robert *et al* 2006, Zhang *et al* 2007, Holm *et al* 2013, Holm and Nasholm 2014), poroelastic models (Biot 1941, 1962, Mow *et al* 1980, 1984, Mak 1986, Miller and Chinzei 1997, Ehlers and Markert 2001, Konofagou *et al* 2001, Righetti *et al* 2004, 2007, Berry *et al* 2006, Cheng and Bilston 2007, Swartz and Fleury 2007, Perrinez *et al* 2009 2010), the linear hysteretic models (Carstensen and Parker 2014, Parker 2014b, at press), polymeric models (Ferry 1970a) and compartmental models (Carstensen and Parker 2014). Recently, the microchannel flow model was introduced to explicitly account for the behavior of tissue as a result of fluid outflow under stress (Parker 2014a). A distribution of vessels and channels leads to a distribution of time constants and an overall relaxation spectrum characterized by a power law parameter. This single parameter then is shown to characterize the frequency distribution of the complex modulus, or stiffness of tissue as a function of frequency. Additional parameters can be introduced to delimit the upper and lower bounds on the distribution of time constants and vessel sizes. This paper extends the previous work by explicitly deriving the mapping function between the branching vasculature and channels, and the relaxation spectrum of the material under uniaxial loading. Then, experimental results from altered samples are compared with predictions from theory. It is found that the resulting changes in tissue responses are reasonably predicted from the microchannel flow model, by considering the changes in fluid flow through the modified samples, and the resulting change in the relaxation spectrum.

The paper is organized as follows: the microchannel flow model is summarized, and then the theory is extended to explicitly account for the mapping function between the channels and the relaxation spectrum. In the results section, the fluid flow properties are modified by temperature and by swelling the tissue. The resulting changes in liver SR responses are found to be close to those predicted from the microchannel flow model. Finally, implications of this study and limitations are discussed.

2. Theory

2.1. Review of theory

The microchannel flow model (Parker 2014a) begins with consideration of a block of liver tissue, comprised of a fine-scale interlocking of hepatic cells, connective tissue, and a variety of fluid channels including billary, capillary, and lymphatic. The hepatocytes and connective tissue are assumed to behave as a homogeneous medium. As a structural element, a cube of tissue is supported at the base and subjected it to uniaxial loading in the *x*-direction (figure 1).

Using conventional notation, σ_x is the stress and ε_x the engineering strain in the *x*-direction. If a steady force F is applied to the upper surface of area A, then $\sigma_x = F/A$. We assume that the idealized tissue block has an elastic component E and that stress is approximately uniform over the element. Next we consider the inclusion of a small fluid microchannel. If the fluid within a microvessel of length L experiences a pressure drop ΔP, then under Poiseuille's Law for incompressible fluids in pipes, a volumetric flow rate Q will result (Sutera 1993).
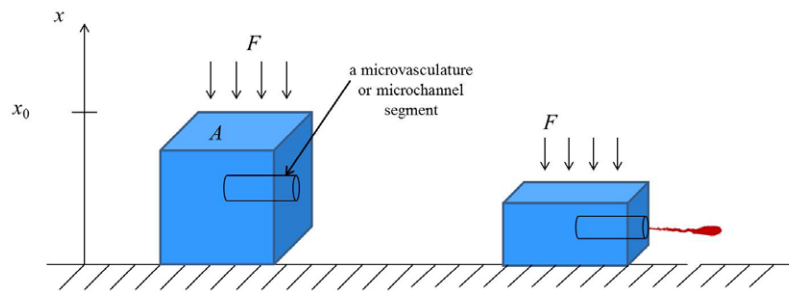
Figure 1. Model of applied stress creating out-flow on an idealized cube of soft tissue with a single vessel.

$$Q = \frac{\Delta P \pi r^4}{\eta 8L},$$ (1)

where r is the radius of the microvessel, η is the viscosity of the fluid, and L is the length of the vessel segment. We then assume that the pressure P_{in} within the sample and microchannel interior is proportional to σ_x and is zero outside the sample. Then the pressure drop ΔP is simply proportional to the applied stress and thus:

$$Q = \frac{C\sigma_x r^4}{\eta},$$ (2)

where C incorporates all previous constants. Here we assume the fluid exits the free boundary shown in figure 1. The loss of fluid volume will result in a loss of volume in of the original cube, and this can be related to the change in height of the block under compression. Assuming negligible change in cross section A, the volume change from the loss of fluid from the sample must be accounted for by a decrease in the x-dimension, or strain ε. Thus,

$$\frac{d\varepsilon_x}{dt} = \frac{Q}{A_0 x_o} = \frac{C\sigma_x r^4}{\eta A_0 x_0},$$ (3)

or

$$\sigma_x = \eta \left(\frac{A_0 x_0}{C r^4} \right) \frac{d\varepsilon_x}{dt},$$ (4)

resembling the equation for a simple dashpot. Now combining elastic and fluid outflow strains as additive leads to a Maxwell model of a series spring and dashpot, therefore the SR curve is a simple exponential decay. If $\varepsilon(t) = \varepsilon_0 U(t)$, where $U(t)$ is the unit step function, then

$$\sigma_{\text{SR}}(t) = \varepsilon_0 E e^{-t/\tau} \text{ for } t \geq 0,$$ (5a)

where the time constant τ is:

$$\tau = \frac{\eta A x_0}{E C r^4}.$$ (5b)

Next, we assume there are multiple microchannels of unequal radius r_n and therefore unequal flow rates Q_n. In this case, if each contributes to the SR at their respective time constant τ_n, then the simplest model for this looks like a parallel set of Maxwell elements (figure 2).
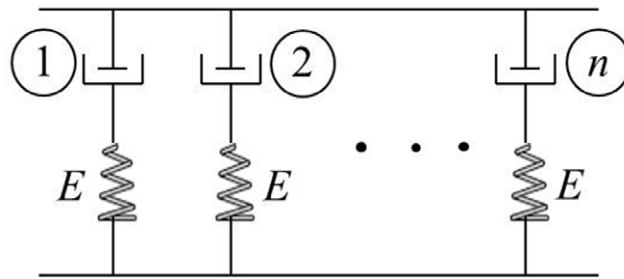
Figure 2. Parallel elements. Each dashpot corresponds to a fluid-filled vessel or channel.

This configuration of multiple parallel elements and an optional single spring element is the generalized Maxwell-Weichert model (Fung 1981a, Ferry 1970b), and in this case it follows directly from the developments of equations (1)–(4). Generally, we can write the SR solution for N Maxwell elements as a Prony series (Lakes 1999), the sum of components with characteristic relaxation time constant τ_N. In the limit, as we allow a continuous distribution of time constants τ, the summation becomes an integral and $A(\tau)$ is the relaxation spectrum, which can be either discrete or continuous, depending on the particular medium under study (Fung 1981a). Given a material's $A(\tau)$, we can write:

$$\sigma_{SR}(t) = \int_{0}^{\infty} A(\tau)e^{-t/\tau}d\tau. \tag{6}$$

Now consider a specific power law distribution:

$$A(\tau) = A_0\tau^{-b}; \quad 1 < b < 2. \tag{7}$$

The power law distribution is naturally occurring in many natural structures including normal and pathological circulatory systems (West *et al* 1997, Risser *et al* 2007). Substituting equation (7) into (6) and solving yields the solution:

$$\sigma_{SR}(t) = A_0 \cdot t^{1-b}\Gamma[b-1] \quad \text{for} \quad 1<b<2, \quad t>0, \tag{8}$$

where Γ is the Gamma function. The SR response is characterized by $1/t^{b-1}$ decay for $t > 0$. For values of $1 < b < 2$ this tends to have a sharp initial drop and then a slow asymptomatic decay. The derivative of the step response yields the impulse response, which defines the basic elastic transfer function for the material. If $\varepsilon(t) = \varepsilon_0\delta(t)$, then

$$\sigma_i(t) = \varepsilon_0 A_0\Gamma[b-1][(1-b)t^{-b}] \quad \text{for} \quad 1<b<2, \quad t>0. \tag{9}$$

For simplicity, let $a = b - 1$ and given the restriction on $1 < b < 2$, then $0 < a < 1$. The impulse response normalized by ε_0 is

$$\sigma_i(t) = A_0\Gamma[a][a/t^{(a+1)}] \quad \text{for} \quad t > 0. \tag{10}$$

The Fourier transform of equation (10) gives the frequency dependence of the complex modulus:

$$E(\omega) = \frac{A_0}{\sqrt{2\pi}}\Gamma[a]\Gamma[1-a]\text{Abs}[\omega]^a\left(\cos\left[\frac{a\pi}{2}\right]+j\text{Sign}[\omega]\sin\left[\frac{a\pi}{2}\right]\right), \tag{11}$$

where $j = \sqrt{-1}$. This response is dominated by the steady increase with frequency to the power of a.

In practical cases it might be realistic to place limits on the range of τ for a material, reflecting the longest and shortest time constraints that pertain to the smallest to largest vessels and microchannels. In this case, the integration of equation (6) has limits $\tau_{\min}$ and $\tau_{\max}$ and

$$\sigma_{SR}(t) = \int_{\tau_{\min}}^{\tau_{\max}} A(\tau)e^{-t/\tau}d\tau, \tag{12}$$

and assuming the power law form of equation (7), then

$$\sigma_{SR}(t) = A_0\left(\frac{\Gamma[a, t/\tau_{\max}] - \Gamma[a, t/\tau_{\min}]}{t^a}\right) \text{for } a > 0, t \geq 0 \text{ and } 0 < \tau_{\min} < \tau_{\max}, \tag{13}$$

where $\Gamma[a, t/\tau]$ is the incomplete Gamma function (upper-tailed). This version of the microchannel flow model is a four parameter model since $\tau_{\max}$ and $\tau_{\min}$ must be determined as material-specific parameters in addition to a and A_0. A different closed form solution exists for cases where $a \leq 1$.

In summary, if a tissue has a power law relaxation spectrum $A(\tau) = \tau^{-b}$, then the SR response will show a $\sigma_{SR} \cong t^{1-b} = 1/t^a$ response. The tissue stress-strain transfer function in the frequency domain is $|E(\omega)| \cong |\omega|^a$. In prostate and liver (Zhang *et al* 2007, Parker 2014a), $0 < a < 1/4$ for many normal specimens.

For a lossless plane shear wave in a homogeneous, nearly incompressible elastic medium, it can be shown that $c_{ph} = \sqrt{E/\rho}$ where ρ is density (Graff 1975, Carstensen and Parker 2014), and in this simple case the speed is constant over any frequency band. More generally, when E is frequency dependent and complex, the complex wave number $\hat{k}$ is given by (Blackstock 2000, Carstensen and Parker 2014):

$$\hat{k} = \frac{\omega}{\sqrt{E(\omega)/\rho}} = \beta - j\alpha, \text{ where } \beta = \frac{\omega}{c_{ph}}, \tag{14}$$

and α is the attenuation, taken from the real and imaginary parts of the $\omega/\sqrt{E(\omega)/\rho}$ term, respectively. For the microchannel flow model, if $|E(\omega)| \propto \omega^{b-1}$, then $c_{ph}^2(\omega) \propto \omega^{b-1}$ also. This was the experimental observation of Zhang *et al* (2007).

2.2. Mapping functions from r to τ

It may seem unlikely that a parallel set of Maxwell elements with uniform values of E as shown in figure 2 can create an $A(\tau)$ in liver of the form $1/\tau^{1.25}$. To illustrate this transformation, consider a tissue block with a discrete set of vessels, one each of $r = 0.2, 0.25...1.0$ mm. According to equations (4)–(5b), the $A(\tau)$ will in that case be discrete and of equal strength but with samples at intervals related to $\tau = c/r^4$ from Poiseuille's law and equation (5b). Figure 3 shows this kind of distribution. One can see that the local density $A(\tau)$ is related to $N(r)$, the relative number of vessels at each radius ($N(r)$ is discrete and uniform in the example of figure 3) and is also dependent on the $1/r^4$ mapping function.

It has long been known that the branching vasculature in soft tissue develops increasing numbers of branches and increasing total cross-sectional area, along the circulation path from major arteries to arterioles then capillaries (Guyton 1971). For branching vasculature, the
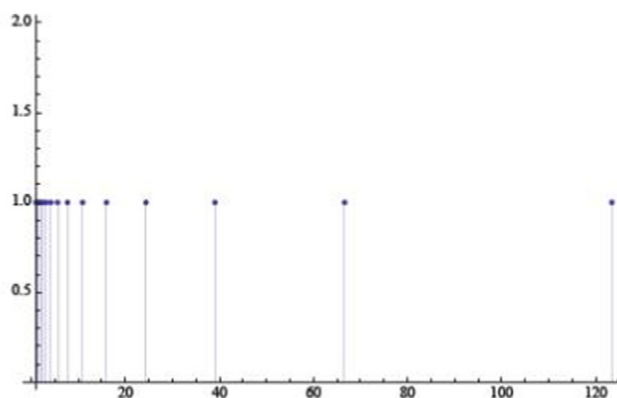
Figure 3. Illustration of how a uniform distribution of vessel radii are transformed to a non-uniform distribution of the relaxation spectrum by a mapping function. The vertical axis is the magnitude of the relaxation spectrum, and the horizontal axis is the time constant τ in seconds. Here the mapping function is related to Poiseuille's law and so the time constant τ in the relaxation spectrum is proportional to $1/r^4$ where r is the radius. In this example, a uniform and discrete set of vessels of radii from 0.2 to 1.0 mm in increments of 0.05 mm are mapped by a $1/r^4$ function to produce the discrete relaxation spectrum which has a much higher local density for small time constants. In the continuous limit, the relaxation spectrum depends on the original distribution of vessels and microchannels, and the mapping function $1/r^4$.

relative number or density function $N(r)$ has been also related to the fractal dimension (Gazit *et al* 1997, West *et al* 1999, Risser *et al* 2007).

Thus, for normal soft tissues such as liver, we can model the general relationship as

$$N(r) = \frac{K}{r^f}, \tag{15}$$

where K is some constant and f is typically less than 3 (Gaudio *et al* 2005), and characterizes the branching nature of the vasculature.

To map this distribution of K/r^f to the relaxation spectrum function $A(\tau)$, we use the general transformation rule from probability theory (Papoulis 1987). Given a monotonic distribution $N(r)$ and a transformation $\tau = g(r) = c/r^4$ from equation (5b), then the transformed density function is given by:

$$A(\tau) = \frac{N(r)}{|dg(r)/dr|}. \tag{16}$$

Substituting equation (15) and taking the derivative of c/r^4, we have

$$A(\tau) = \frac{(K/r^f)}{(4c/r^5)} = A_0 r^{5-f} = A_0 \left(\frac{c}{\tau}\right)^{\left(\frac{5-f}{4}\right)}, \tag{17}$$

where $A_0 = K/4c$. Thus, comparing with equation (7), the 'master' power law parameter b of the relaxation spectrum is driven by the vascular f parameter and the Poiseuille's law transformations so that $b = (5 - f)/4$. Note that for values of f near 1 (i.e. when $N(r) \approx K/r^1$), then $A(\tau)$ approaches $1/\tau^1$. This represents the limit of convergence of equations (6)–(8), but also represents a zone where the phenomenon of 'linear hysteresis' would be observed (Parker, 2015). This can be seen in equation (11) when the related parameter $a \to \varepsilon$ then the complex
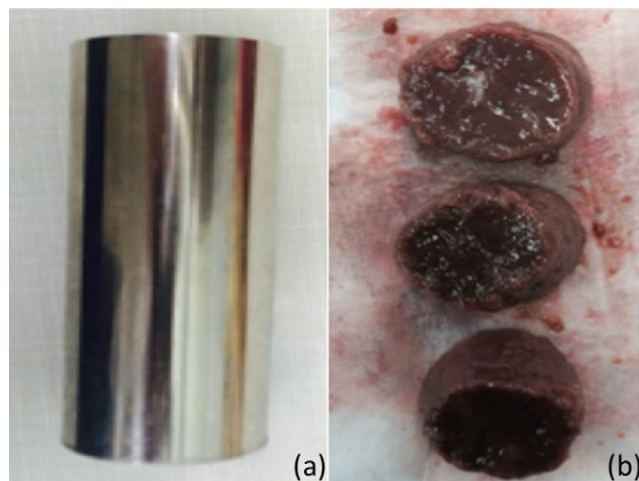
Figure 4. (a) Cylindrical metal tool that is used to cut tissue and cores. (b) Sample of beef liver tissue soaked overnight in 0.9% saline.

modulus is nearly independent of frequency which is the hallmark of 'linear hysteresis.' For larger values of f the limited form of the integral is required for convergence, implying the use of equation (12) and its explicit solutions for $b < 1$.

3. Methods

Experimental tests of the microchannel flow model were made on liver samples where changes in salinity or temperature were found to change the SR curves.

Whole fresh veal (bovine) livers were obtained from a slaughterhouse and were place on ice for transport to our laboratories. Cylindrical cores (approximately 25 mm in diameter and 60 mm in length) were acquired from the livers using a custom-made coring knife as shown in figure 4.

Nine cylindrical samples of approximately 16 mm in length were cut from the cores and carefully selected to avoid large scale vessels or ligaments. These were divided into three groups of three each, stored at 4 °C for 24 h in either hypotonic (0.65%) saline, normal (0.9%) saline, or hypertonic (1.15%) saline. The osmotic pressure difference can cause swelling or shrinking, and the general effect of hypotonic swelling is depicted in figure 5.

A 1/S mechanical device (MTS Systems Co., Eden Prairie, MN, USA) with a 5 Newton load cell was used to test the core samples. The upper and lower plates were coated with vegetable oil before testing. The core samples were put on the center of the lower testing plate. The top plate was used as a compressor and carefully positioned to fully contact the sample. After two minutes for tissue recovery, the uniaxial unconfined compression controlled by TestWorks 3.10 software (Software Research, Inc., San Francisco, CA, USA) was conducted to measure the time domain SR data at room temperature. Throughout the test, the stress required to maintain the compression was recorded over time, approximately 700 s. The resulting data consisted of a plot of the stress versus time under 10% strain.

The SR curve of each sample during the hold period was fitted to the microchannel flow model using the MATLAB (The MathWorks, Inc., Natick, MA, USA) curve fitting toolkit. The trust-region method for nonlinear least squares fitting was applied on each curve.
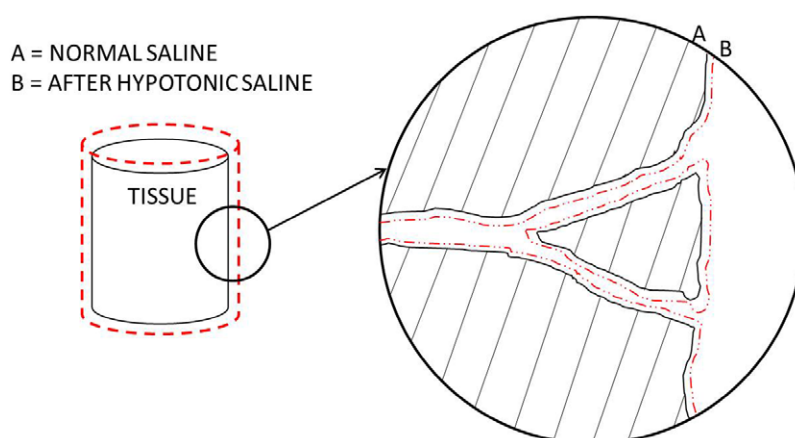
Figure 5. Schematic of liver tissue, illustrating a core sample with vessels in normal state after storage and refrigeration in normal saline, and alternatively the liver sample in a 'swollen' state after storage in hypotonic saline. The swelling of hepatocytes results in a reduction in the radii of the smaller vasculature and microchannels. This has major effects on the SR response of the tissue core samples.

4. Results

4.1. Modifications from hyper- or hypotonic storage

Figure 6 shows the raw and fitted curve of an average of three beef liver specimens that were soaked overnight at 0.65% (hypotonic) saline concentration. Figure 6(a) represents the graph obtained by using a three parameter Kelvin–Voigt fractional derivative (KVFD) model where the higher curve (at 50 s) represents the SR of raw data and the lower curve (at 50 s) is the fitted curve approximated by the KVFD model. Likewise, figure 6(b) shows the raw data and fitted curve using a microchannel flow model with four parameters, equation (13). The result shows that the four parameter model provides us with a closer curve fit for the beef liver tissues compared to the KVFD model. However, it should be understood that in general the addition of a fourth parameter adds a degree of freedom and therefore would be expected to improve curve fitting.

The summary of the four parameters microchannel flow model of the beef liver tissues in different saline concentrations is illustrated in figure 7.

In the four parameter model parameters, the amplitude *A* has a distinct trend as its value is decreasing from 0.65% saline (highest) to 1.15% saline (lowest). $\tau_{\min}$ is the lower limit of the relaxation spectrum and it seems $\tau_{\min}$ values are similar for 0.65% and 1.15% saline concentration. $\tau_{\max}$ is the upper limit of the spectrum amplitude. Numerical values are given in table 1. All parameters should be considered to be approximate, as will be detailed in the Discussion.

A theoretical perspective on these results is given in appendix 2.

4.2. Viscosity/temperature

As an independent experimental test of the microchannel flow model, liver specimens' shear wave velocities were measured using the 'crawling wave' methods (Wu *et al* 2006, Barry *et al* 2012, Barry *et al* 2014) over a range of temperatures from 7 to 17 °C. Temperature changes the fluid viscosity in a monotonic relationship. The shear wave measurements are
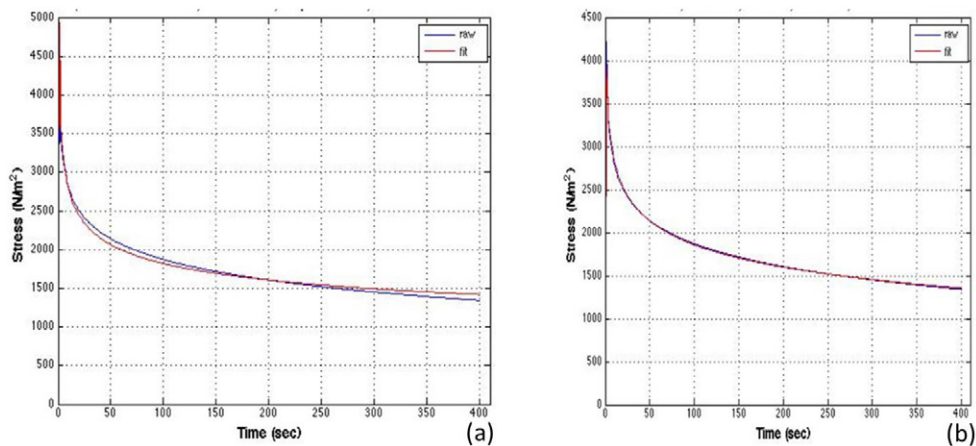
Figure 6. Hypotonic liver SR curves. (a) The higher curve (at 50 s) shows the SR curve of beef liver tissue and the lower curve (at 50 s) shows the curve fitting using KVFD model. (b) Curve-fitting using microchannel flow model. The raw data of SR and the curve-fitting using four parameters model are both shown; however they overlap substantially and appear as a single curve.
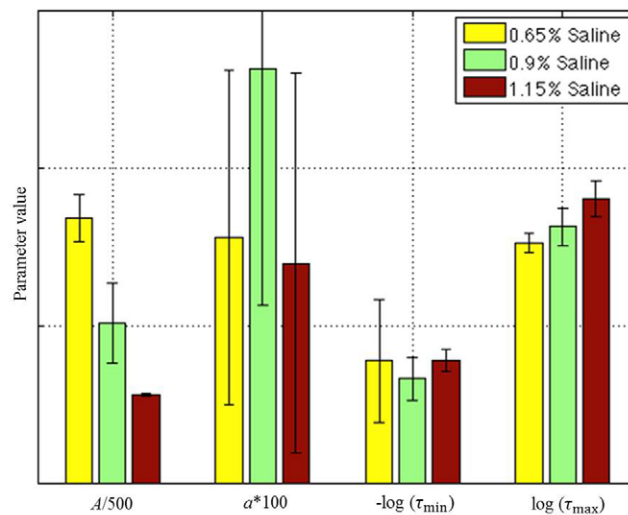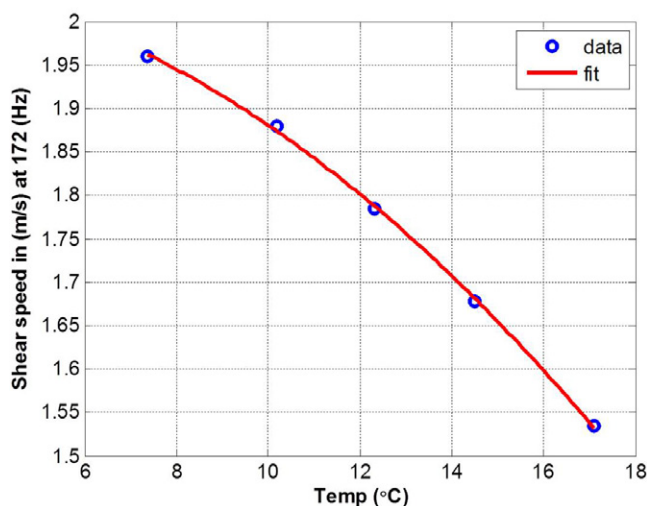

Figure 7. The value of SR curve fit parameters of beef liver tissue in different saline concentrations, 0.65% saline, 0.9% saline, and 1.15% saline. After storage in hypotonic saline, the swollen livers appear more 'stiff' than the other groups, as shown by the left set of bars representing the overall magnitude '*A*'. The parameters *A* and *a* have been scaled, while $-\log(\tau_{min})$ and $\log(\tau_{max})$ are shown so that all parameters fall within a common scale.

shown in figure 8. Theoretically, the SR time constant is linked to the fluid viscosity by equations (4) and (5b). Furthermore, if the viscosity of the fluid is increased by a factor of *m*, then the resulting stiffness will increase as m^b, as demonstrated in appendix 1.

Assuming in our case that the liver specimens' fluids at 7 °C have a viscosity near 6 cp, while the liver fluids at 17 °C are approximately 4.3 cp based on values of saline and blood

Table 1. Four parameter model estimates for beef liver soaked in different % of saline: average of three samples.

Beef liver saline %	A (magnitude Pa·s^a)	a (power law dimension)	τ_{min} (lower limit ms)	τ_{max} (upper limit seconds)	Average length (mm)	Average diameter (mm)
0.65	4.1×10^3	0.11	6.7	1.8×10^4	15.2	27.4
0.9	2.5×10^3	0.14	17	2.7×10^4	17.7	26.6
1.15	1.4×10^3	0.11	11	4.9×10^4	18	25.9

Figure 8. Shear wave speed in *ex vivo* liver versus temperature. Data are derived from shear wave propagation experiments taken at mid-band, 172 Hz shear wave frequency. The solid line represents a second order polynomial fit where speed c (m s^{-1}) is a function of temperature T (°C): $c(T) = 2.05 + 0.0012T - 0.0019T^2$.

from Stammers *et al* (2003) and Ozbek (1971), then the colder specimens should appear stiffer by a factor of $(6 / 4.3)^b$ or roughly $(6 / 4.3)^{1.25} = 1.5$.

The ratio of shear waves (squared to convert to E) is from figure 3: $(1.96 / 1.53)^2 = 1.6$. The ratio of 1.6 is consistent with the hypothesis of the effects of increasing fluid viscosity on tissue stiffness using the microchannel flow model. Furthermore, it was found that the power law a (related to the dispersion of crawling waves) remained near 0.24 as would be predicted by consideration of the equations in appendix 1. It is possible that the estimated viscosity values are not accurate, and that the elastic polymers in tissue by themselves exhibit a similar temperature dependence. Other complicating factors are discussed in the next section.

5. Discussion

5.1. The distribution of microchannels and resulting dispersion.

In the derivation of the microchannel flow model, the parameter f that describes the number density of the vasculature and channels, ultimately sets the relaxation spectrum $A(\tau)$ (see equation (17)) and therefore the frequency dependent term of the modulus: ω^a where $a = 1 - (5 - f)/4$. This implies that the frequency dependent modulus can never increase

faster than $\omega^{0.25}$ unless either f is negative or the strict assumptions of the derivation, including Poiseuille's law, are violated below some characteristic dimension. For example, the single parameter f may be appropriate for describing the branching vasculature; however the liver has many microchannel systems and fluid-filled gaps at smaller dimensions. These include the space of Mall, the space of Disse, and the intercellular bile canaliculi which are less than a micron in diameter (Clearfield 1965). Thus it is possible that the single f parameter would, in practice, need to be modified to encompass the smallest level of microchannels, corresponding to the longest time constants.

Another possibility not considered in the microchannel flow model is the addition of highly viscous material to the liver tissue, as could be found in the development of simple steatosis (Barry *et al* 2015, at press). In this case an additional 'dashpot' or lossy mechanism would be required to model the additional component not accounted for in the derivation of the microchannel flow model.

5.2. Predictions for changes in tissue response

The microchannel flow model predicts a number of ways in which a sample of normal soft tissue such as liver can be modified so as to be perceived as less compliant, or hardened. First, any increase in the underlying elastic response characterized by E in figure 2 would increase the overall amplitude of the SR response, according to equations (5a)–(6). However, the time constants in the relaxation spectrum would be shifted to the left (shorter time constants) according to equation (5b), so the overall change would be most dramatic early in the SR curve. An increase in E may, for example, be achieved by soaking the specimens in formalin, which is known to harden and preserve samples. A second way to harden a sample is less intuitive. As the viscosity of the fluids in the microchannels increases, the resulting SR forces will increase according to the derivation of appendix 1. This could apply to experiments where the temperature is changed (within limits of avoiding chemical or phase changes), or where the fluid is replaced by blood substitutes. Finally, and even less obvious is the hardening caused by constriction of the smallest microchannels. This has a double effect in modifying the relaxation spectrum, and shifting it to the right (longer time constants) according to the derivation of appendix 2. The net result is a modification that makes the specimen feel more resistant or harder, over long time intervals. This was experimentally approximated with swelling from hypotonic saline; however *in vivo* this could be the net effect of inflammatory responses or edema. This could explain, for example, why inflamed regions of skin feel harder than the surrounding normal tissue.

5.3. Relation to other models

It should be noted that the power law behavior exhibited by equation (11) has been noted in different materials (Lakes 1999), and can be modeled by a number of theoretical approaches. A key element is the concept of multiple mechanisms operating across a range of scales or time constants (Fung 1981b, Liu and Bilston 2000). Multi-scale ladders or mechanisms can be modeled by the fractional derivative operators (Sokolov *et al* 2002), and the microchannel flow two-parameter model resembles the KVFD model with $E_0 = 0$ (Parker 2014a). Other models have been derived from the application of fractional derivative operators (Holm and Nasholm 2014) in the wave equation. Alternatively, the power law behavior of viscoelastic tissues were recently linked to the architecture of tissue, particularly cross-linked or entangled microstructures (Guo *et al* 2012, Sack *et al* 2013). For any particular tissue, especially

pathological tissues, careful determination will be required to identify the dominant mechanisms that contribute to observed behavior.

5.4. Limitations of the model and study

The derivation of the microchannel flow model includes a number of assumptions that may not be rigorously true in normal soft tissues. All constants from equations (1)–(8), and then the branching vasculature or fluid channel parameter f are assumed to be strictly constant across all radii, including the fundamental $1/r^4$ proportionality imposed by Poiseuille's law. These may in practice require some adjustment especially at smaller scales down to channels of only a few microns. Furthermore, there are no dynamic or inertial terms in the derivation. This could be required, for example, in higher frequency shear wave propagation, where eventually an ω^2 term would be required to fully account for fluid acceleration in the microchannels. Further research is necessary to better define this transition.

A practical limitation of the four channel model is the lack of accuracy and uniqueness of estimated parameters from limited data. For example, experimental SR data from one to 500 s can be curve fit to the four parameter model, equation (13), to obtain estimated parameters (A, a, τ_{min}, and τ_{max}) such as those shown in table 1. However, the data will include noise and imperfections such as drift, temperature fluctuations, and shape distortions from cutting the sample. This creates uncertainties in the estimations as in all parameter estimation schemes. As a specific example, consider an ideal specimen described perfectly by the parameters: (1000, 0.2, 1/333, 71 000). It can easily be shown that the SR curve between 10 and 500 s for another specimen defined by (1050, 0.2, 1/333, 50 000) is very similar to the first specimen, differing by less than 4% over the curves from 10 to 500 s. Here the first parameter (overall magnitude A) and the last parameter (τ_{max}) are seen to 'trade off', at least over some limited period of observation of the responses. Thus, given the presence of noise and imperfections, our ability to precisely determine the four parameters is limited. However, the parameters still can serve a useful purpose in providing an analytical model for soft tissue and their rough estimates provide useful predictions of behavior across a range of practical circumstances.

6. Conclusion

The microchannel flow model focuses on fluid flow in tissues through a range of channels in response to applied stress. A power law relation of branching vasculature and channels versus size is transformed by Poiseuille's law into a power law relaxation spectrum. This leads to a SR response of tissue that is dominated by a power law function of time, which can also be modified by terms relating to the maximum and minimum time constants that are present in the tissue. Experimental tests of normal liver tissue subjected to hypo- or hypertonic solutions or alternatively to temperature variations demonstrate the resulting changes in tissue stiffness can be reasonably predicted by application of the microchannel flow model. In addition, the model illustrates a potentially important effect whereby constriction of the smallest channels due to tissue edema can strongly increase the maximum time constant τ_{max}, and that directly increases the SR response, and the perceived stiffness or hardness of the affected tissue.

Acknowledgments

Appendix 1

The dependence of a sample on viscosity can be shown by examining the basic equations (4)–(8). If we assume that $A(\tau_1)$ of tissue specimen '1' is related to the distribution and geometry of the microchannels, then replace the specimen's fluids with a substitute of higher viscosity $\eta_2 = m \cdot \eta_1$ where $m > 1$; then the new relaxation spectrum is $A(\tau_2 / m)$. For example, if $m = 3$, then the original value of $A(\tau_1 = 1)$ now corresponds to the relaxation spectrum value at $\tau_2 = 3$ in the sample '2' with the higher viscosity substitute. Accordingly, if, following equations (6) and (7), we substitute:

$$\sigma_{SR_2}(t) = \int_0^\infty A_0\left(\frac{\tau_2}{m}\right)^{-b} e^{(-t/\tau_2)} d\tau_2 \tag{A.1}$$
$$= (m^b)\sigma_{SR_1}(t).$$

In other words, the sample with higher viscosity fluid would appear stiffer by a factor of m^b but would have the same power law time constant.

Appendix 2

In this derivation we examine the change in SR due to change in vessel and microchannel radius. Assume that a 24 h soak in hypotonic (0.65%) saline creates a swelling and therefore a strain ε of hepatocytes in an *ex vivo* specimen, as shown in figure 4. We assume the specimen's initial relaxation spectrum is $A(\tau) = A_0/\tau^b$ and it has a vessel distribution of $N_0(r)$. After swelling, we further assume a simplified model of the effect, where all radii after hypotonic swelling, r_2, are reduced by

$$r_2 = r - \Delta r. \tag{A.2}$$

Given $N_0(r) = K_0/r^f$, and $N_2(r_2) = K_0/(r_2 + \Delta r)^f$, and from equations (16) and (17):

$$A_2(\tau) = A_0\left(\frac{c}{\tau}\right)^{5/4}\left(\frac{1}{(c/\tau)^{1/4} + \Delta r}\right)^f \tag{A.3}$$

$$= A(\tau)\left(\frac{1}{1 + \Delta r(\tau/c)^{1/4}}\right)^f. \tag{A.4}$$

So the new relaxation spectrum $A_2(\tau)$ is based on the original tissue's $A(\tau)$; modified and somewhat diminished by a factor, the final term in equation (A.4). However, the limits of integration over the time constants in equation (12) must also change. The original tissue limits, τ_{min} to τ_{max} are now modified since r_{max} is now $r_{max} - \Delta r$ in the swollen tissue and r_{min} is now $r_{min} - \Delta r$. In some cases, the small change in r_{max} is insignificant, so τ_{min} remains approximately the same. However, when $\Delta r \approx r_{min}$ (which can be on a micron scale), then as $r_{min} - \Delta r \to 0$, the maximum time constant $\tau_{max} \to \infty$, and this results in a major shift in the behavior of the material.

As an example of this phenomenon, figure 9 demonstrates SR curves for a set of parameters consistent with the liver values of table 1, where the lower curve represents a normal liver
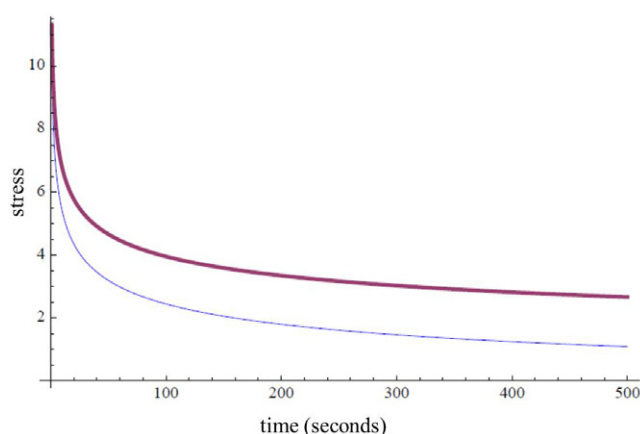
Figure 9. SR curves for a set of parameters consistent with the liver values of table 1. The lower curve represents a normal liver and the upper (thick) curve represents the specimen after some constriction of the microchannels due to swelling of the parenchymal cells. The four parameter microchannel flow model was used in each case but with upper limit of the relaxation spectrum taken as 4000 s in the normal case. For the second case, the relaxation spectrum upper limit was adjusted up to 1.6×10^7 s, corresponding to a significant reduction of radius of the smallest available microchannels or vessels. In this case, the second sample would be perceived as the harder material.

and the upper (thick) curve represents the specimen after some constriction of the microchannels due to swelling of the parenchymal cells. In this example, $A_0 = 7000$ Pa·s, $f = 0.2$, $c = 10^{-14}$ m^4 s, and $\Delta r = 35\,\mu$m. Numerical integration was performed of equation (12) using equation (17) for the normal tissue and $\tau_{min} = 0.01$ and $\tau_{max} = 4000$ s. For the second case, numerical integration was performed using equation (A.4), but with $\tau_{max} = 1.6 \times 10^7$ s, corresponding to a reduction in minimum channel to $5\,\mu$m. The slight reduction in the relaxation spectrum is more than compensated for by the extended upper limit of integration over τ, and the result is a higher net SR response. In this case, the second sample would be perceived as the harder material.

References

Bagley R L and Torvik P J 1983 A theoretical basis for the application of fractional calculus to viscoelasticity *J. Rheol.* **27** 201–10

Barry C T, Hah Z, Partin A, Mooney R A, Chuang K-H, Augustine A, Almudevar A, Cao W, Rubens D J and Parker K J 2014 Mouse liver dispersion for the diagnosis of early-stage fatty liver disease: a 70-sample study *Ultrasound Med. Biol.* **40** 704–13

Barry C T, Hazard C, Hah Z, Cheng G, Partin A, Mooney R A, Chuang K, Cao W, Rubens D J and Parker K J 2015 Shear wave dispersion in lean vs. steatotic rat livers *J. Ultrasound Med.* at press

Barry C T, Mills B, Hah Z, Mooney R A, Ryan C K, Rubens D J and Parker K J 2012 Shear wave dispersion measures liver steatosis *Ultrasound Med. Biol.* **38** 175–82

Bercoff J, Tanter M, Muller M and Fink M 2004 The role of viscosity in the impulse diffraction field of elastic waves induced by the acoustic radiation force *IEEE Trans. Ultrason. Ferroelectr. Freq. Control* **51** 1523–36

Berry G P, Bamber J C, Armstrong C G, Miller N R and Barbone P E 2006 Towards an acoustic model-based poroelastic imaging method: I. Theoretical foundation *Ultrasound Med. Biol.* **32** 547–67

Biot M A 1941 General theory of 3D consolidation *J. Appl. Phys.* **12** 155–64

Biot M A 1962 Mechanics of deformation and acoustic propagation in porous media *J. Appl. Phys.* **33** 1482–98

Blackstock D T 2000 *Fundamentals of Physical Acoustics* (New York: Wiley)

Caputo M 1967 Linear models of dissipation whose q is almost frequency dependent: II *Geophys. J. R. Astron. Soc.* **13** 529–39

Carstensen E L and Parker K J 2014 Physical models of tissue in shear fields *Ultrasound Med. Biol.* **40** 655–74

Catheline S, Gennisson J L, Delon G, Fink M, Sinkus R, Abouelkaram S and Culioli J 2004 Measurement of viscoelastic properties of homogeneous soft solid using transient elastography: an inverse problem approach *J. Acoust. Soc. Am.* **116** 3734–41

Chen S, Fatemi M and Greenleaf J F 2004 Quantifying elasticity and viscosity from measurement of shear wave speed dispersion *J. Acoust. Soc. Am.* **115** 2781–5

Chen S, Urban M W, Pislaru C, Kinnick R, Zheng Y, Yao A and Greenleaf J F 2009 Shearwave dispersion ultrasound vibrometry (SDUV) for measuring tissue elasticity and viscosity *IEEE Trans. Ultrason. Ferroelectr. Freq. Control* **56** 55–62

Chen S G *et al* 2013a Assessment of liver viscoelasticity by using shear waves induced by ultrasound radiation force *Radiology* **266** 964–70

Chen X, Shen Y Y, Zheng Y, Lin H M, Guo Y R, Zhu Y, Zhang X Y, Wang T F and Chen S P 2013b Quantification of liver viscoelasticity with acoustic radiation force: a study of hepatic fibrosis in a rat model *Ultrasound Med. Biol.* **39** 2091–102

Cheng S and Bilston L E 2007 Unconfined compression of white matter *J. Biomech.* **40** 117–24

Clearfield H R 1965 *Gastroenterology* vol 3 (Philadelphia, PA: Saunders) chapter 89

Delingette H 1998 Toward realistic soft-tissue modeling in medical simulation *Proc. IEEE* **86** 512–23

Doyley M M 2012 Model-based elastography: a survey of approaches to the inverse elasticity problem *Phys. Med. Biol.* **57** R35–73

Ehlers W and Markert B 2001 A linear viscoelastic biphasic model for soft tissues based on the theory of porous media *Trans. ASME, J. Biomech. Eng.* **123** 418–24

Ferry J D 1970a *Viscoelastic Properties of Polymers* (New York: Wiley)

Ferry J D 1970b *Viscoelastic Properties of Polymers* (New York: Wiley) chapter 1

Fung Y C 1981a *Biomechanics: Mechanical Properties of Living Tissues* (New York: Springer) chapter 2

Fung Y C 1981b *Biomechanics: Mechanical Properties of Living Tissues* (New York: Springer) chapter 7

Gaudio E, Chaberek S, Montella A, Pannarale L, Morini S, Novelli G, Borghese F, Conte D and Ostrowski K 2005 Fractal and Fourier analysis of the hepatic sinusoidal network in normal and cirrhotic rat liver *J. Anat.* **207** 107–15

Gazit Y, Baish J W, Safabakhsh N, Leunig M, Baxter L T and Jain R K 1997 Fractal characteristics of tumor vascular architecture during tumor growth and regression *Microcirculation* **4** 395–402

Gennisson J L, Lerouge S and Cloutier G 2006 Assessment by transient elastography of the viscoelastic properties of blood during clotting *Ultrasound Med. Biol.* **32** 1529–37

Giannoula A and Cobbold R S C 2009 Propagation of shear waves generated by a modulated finite amplitude radiation force in a viscoelastic medium *IEEE Trans. Ultrason. Ferroelectr. Freq. Control* **56** 575–88

Graff K F 1975 *Wave Motion in Elastic Solids* (Oxford: Clarendon)

Guo J, Posnansky O, Hirsch S, Scheel M, Taupitz M, Braun J and Sack I 2012 Fractal network dimension and viscoelastic powerlaw behavior: II. An experimental study of structure-mimicking phantoms by magnetic resonance elastography *Phys. Med. Biol.* **57** 4041–53

Guyton A C 1971 *Textbook of Medical Physiology* (Philadelphia, PA: Saunders)

Holm S and Nasholm S P 2014 Comparison of fractional wave equations for power law attenuation in ultrasound and elastography *Ultrasound Med. Biol.* **40** 695–703

Holm S, Näsholm S P, Prieur F and Sinkus R 2013 Deriving fractional acoustic wave equations from mechanical and thermal constitutive equations *Comput. Math. Appl.* **66** 621–9

Humphrey J D 2003 Continuum biomechanics of soft biological tissues *Proc. R. Soc.* A **459** 3–46

Kiss M Z, Varghese T and Hall T J 2004 Viscoelastic characterization of *in vitro* canine tissue *Phys. Med. Biol.* **49** 4207–18

Klatt D, Hamhaber U, Asbach P, Braun J and Sack I 2007 Noninvasive assessment of the rheological behavior of human organs using multifrequency MR elastography: a study of brain and liver viscoelasticity *Phys. Med. Biol.* **52** 7281–94

Konofagou E E, Harrigan T P, Ophir J and Krouskop T A 2001 Poroelastography: imaging the poroelastic properties of tissues *Ultrasound Med. Biol.* **27** 1387–97

Lakes R S 1999 *Viscoelastic Solids* (Boca Raton, FL: CRC) chapter 2

Liu Z and Bilston L 2000 On the viscoelastic character of liver tissue: experiments and modelling of the linear behaviour *Biorheology* **37** 191–201

Mak A F 1986 Unconfined compression of hydrated viscoelastic tissues: a biphasic poroviscoelastic analysis *Biorheology* **23** 371–83

Miller K and Chinzei K 1997 Constitutive modelling of brain tissue: experiment and theory *J. Biomech.* **30** 1115–21

Mow V C, Holmes M H and Lai W M 1984 Fluid transport and mechanical properties of articular cartilage: a review *J. Biomech.* **17** 377–94

Mow V C, Kuei S C, Lai W M and Armstrong C G 1980 Biphasic creep and stress relaxation of articular cartilage in compression? Theory and experiments *J. Biomech. Eng.* **102** 73–84

Ozbek H 1971 Viscosity of aqueous sodium chloride from 0–150°C *American Chemical Society 29th Southease Regional Meeting (Tampa, FL)* pp 1–67

Papoulis A 1987 *The Fourier Integral and its Applications* (New York: McGraw-Hill)

Parker K J 2014a A microchannel flow model for soft tissue elasticity *Phys. Med. Biol.* **59** 4443–57

Parker K J 2014b Real and causal hysteresis elements *J. Acoust. Soc. Am.* **135** 3381–9

Parker K J 2015 Could linear hysteresis contribute to shear wave losses in tissues? *Ultrasound Med. Biol.* **41** 1100–4

Parker K J, Doyley M M and Rubens D J 2011 Imaging the elastic properties of tissue: the 20 year perspective *Phys. Med. Biol.* **56** R1–29

Perrinez P R, Kennedy F E, Van Houten E E, Weaver J B and Paulsen K D 2009 Modeling of soft poroelastic tissue in time-harmonic MR elastography *IEEE Trans. Biomed. Eng.* **56** 598–608

Perrinez P R, Kennedy F E, Van Houten E E, Weaver J B and Paulsen K D 2010 Magnetic resonance poroelastography: an algorithm for estimating the mechanical properties of fluid-saturated soft tissues *IEEE Trans. Med. Imaging* **29** 746–55

Righetti R, Ophir J, Srinivasan S and Krouskop T A 2004 The feasibility of using elastography for imaging the Poisson's ratio in porous media *Ultrasound Med. Biol.* **30** 215–28

Righetti R, Righetti M, Ophir J and Krouskop T A 2007 The feasibility of estimating and imaging the mechanical behavior of poroelastic materials using axial strain elastography *Phys. Med. Biol.* **52** 3241–59

Risser L, Plouraboue F, Steyer A, Cloetens P, Le Duc G and Fonta C 2007 From homogeneous to fractal normal and tumorous microvascular networks in the brain *J. Cerebr. Blood Flow Metabolism* **27** 293–303

Robert B, Sinkus R, Larrat B, Tanter M and Fink M 2006 A new rheological model based on fractional derivatives for biological tissues *IEEE Ultrasonics Symp., 2006* pp 1033–6

Sack I, Johrens K, Wurfel J and Braun J 2013 Structure-sensitive elastography: on the viscoelastic powerlaw behavior of *in vivo* human tissue in health and disease *Soft Matter* **9** 5672–80

Samani A, Zubovits J and Plewes D 2007 Elastic moduli of normal and pathological human breast tissues: an inversion-technique-based investigation of 169 samples *Phys. Med. Biol.* **52** 1565–76

Sokolov I M, Klafter J and Blumen A 2002 Fractional kinetics *Phys. Today* **55** 48–54

Stammers A H, Vang S N, Mejak B L and Rauch E D 2003 Quantification of the effect of altering hematocrit and temperature on blood viscosity *J. Extra Corpor. Technol.* **35** 143–51

Suki B, Barabasi A L and Lutchen K R 1994 Lung-tissue viscoelasticity: a mathematical framework and its molecular basis *J. Appl. Physiol.* **76** 2749–59

Sutera S P 1993 The history of Poiseuille's law *Annu. Rev. Fluid Mech.* **25** 1–19

Swartz M A and Fleury M E 2007 Interstitial flow and its effects in soft tissue *Annu. Rev. Biomed. Eng.* **9** 229–56

Taylor L S, Richards M S and Moskowitz A J 2001 Viscoelastic effects in sonoelastography: impact on tumor detectability *IEEE Ultrasonics Symp., 2001* pp 1639–42

Walker W F, Fernandez F J and Negron L A 2000 A method of imaging viscoelastic parameters with acoustic radiation force *Phys. Med. Biol.* **45** 1437–47

West G B, Brown J H and Enquist B J 1997 A general model for the origin of allometric scaling laws in biology *Science* **276** 122–6

West G B, Brown J H and Enquist B J 1999 The fourth dimension of life: fractal geometry and allometric scaling of organisms *Science* **284** 1677–9

Wu Z, Hoyt K, Rubens D J and Parker K J 2006 Sonoelastographic imaging of interference patterns for estimation of shear velocity distribution in biomaterials *J. Acoust. Soc. Am.* **120** 535–45

Zhang M, Castaneda B, Wu Z, Nigwekar P, Joseph J V, Rubens D J and Parker K J 2007 Congruence of imaging estimators and mechanical measurements of viscoelastic properties of soft tissues *Ultrasound Med. Biol.* **33** 1617–31